

Two-gap superconductivity in heavily n -doped graphene: *ab initio* Migdal-Eliashberg theory

E. R. Margine^{1,*} and Feliciano Giustino^{2,†}

¹*Department of Physics, Applied Physics and Astronomy,
Binghamton University - SUNY, Binghamton, New York 13902, USA*

²*Department of Materials, University of Oxford, Parks Road, Oxford OX1 3PH, United Kingdom*

Graphene is the only member of the carbon family from zero- to three-dimensional materials for which superconductivity has not been observed yet. At this time, it is not clear whether the quest for superconducting graphene is hindered by technical challenges, or else by the fluctuation of the order parameter in two dimensions. In this area, *ab initio* calculations are useful to guide experimental efforts by narrowing down the search space. In this spirit, we investigate from first principles the possibility of inducing superconductivity in doped graphene using the fully anisotropic Migdal-Eliashberg theory powered by Wannier-Fourier interpolation. To address a best-case scenario, we consider both electron and hole doping at high carrier densities, so as to align the Fermi level to a van Hove singularity. In these conditions, we find superconducting gaps of s -wave symmetry, with a slight anisotropy induced by the trigonal warping, and, in the case of n -doped graphene, an unexpected two-gap structure reminiscent of MgB_2 . Our Migdal-Eliashberg calculations suggest that the observation of superconductivity at low temperature should be possible for n -doped graphene at carrier densities exceeding 10^{15}cm^{-2} .

I. INTRODUCTION

Superconductivity in lightweight carbon-based materials was first discovered almost half a century ago in alkali-metal doped graphite¹. Since then, the intercalation of metal atoms into graphite and fullerene solids has led to superconducting critical temperatures T_c above 11 K in CaC_6 at ambient pressure² and 38 K in Cs_3C_{60} under applied pressure³. Substitutional doping of diamond with boron also induces a superconducting state, with a critical temperature in the range 4-10 K^{4,5}. The most recent breakthroughs within the family of carbon-based materials are the discoveries of superconductivity in doped polycyclic aromatic hydrocarbons, namely picene⁶, phenanthrene⁷, coronene⁸, and dibenzopentacene⁹, with critical temperatures up to 33 K⁹.

The discovery of graphene^{10,11} together with its unique properties^{12,13} immediately raised the question of whether superconductivity could be achieved also in this two-dimensional material. Within this context, theoretical studies explored both conventional and unconventional pairing mechanisms¹⁴⁻¹⁹. In the former case, it was suggested that phonon-mediated superconductivity could be induced by tailoring the electron-phonon coupling (EPC) via alkali-metal doping¹⁵. In the latter case, it was proposed that chiral superconductivity should arise when graphene is doped near the van Hove singularity (VHS), as a result of strong electron-electron interactions^{18,19}. Chemical modifications of graphene were also predicted to lead to superconductivity. For example, in close analogy to B-doped diamond⁴, hole-doped graphene²⁰ was predicted to be a high- T_c superconductor²¹.

Despite such a variety of theoretical predictions, so far none has been confirmed experimentally. This raises the question of whether there exists a fundamental limi-

tation preventing a superconducting phase transition in graphene, similar to the Mermin-Wagner theorem²², or if inducing and observing superconductivity is indeed possible but technically very challenging.

On the experimental front, the study of possible pairing mechanisms is complicated by the sensitivity of the EPC to the character and location of the metal atoms, as well as the underlying substrates²³⁻²⁶. For example, the EPC strength determined by angle-resolved photoelectron spectroscopy differs substantially in the cases of sub-surface intercalation of potassium on graphene/Au²⁶ and potassium adsorption on graphene/Ir²⁴. This sensitivity may reflect the substrate-induced modification of the electronic structure in proximity of the Dirac point: for example, graphene on Ir or Cu exhibits a band gap^{24,25}, graphene grown on Au is gapless²⁶, and in the case of SiC both situations have been reported^{23,27}.

Given the lack of experimental confirmation of current theories, and the difficulty in extracting the relevant pairing parameters from experiment, in order to understand the potential of graphene for superconductivity it is important to carry out careful investigations using the most advanced tools available.

In this work we study from first principles the possibility of superconductivity in heavily doped graphene. We employ a recent *ab initio* implementation of the anisotropic Migdal-Eliashberg theory^{28,29} based on electron-phonon Wannier-Fourier interpolation^{30,31}. This technique allows us to describe the electron-phonon pairing mechanism by taking fully into account the highly anisotropic nature of graphene, and by sampling the Brillouin zone with unprecedented accuracy. By considering high carrier densities, whereby the Fermi energy approaches a VHS, we show below that superconductivity should be attainable at least in n -doped graphene, due to the additional pairing channels associated with the free-electron-like (FEL) band.

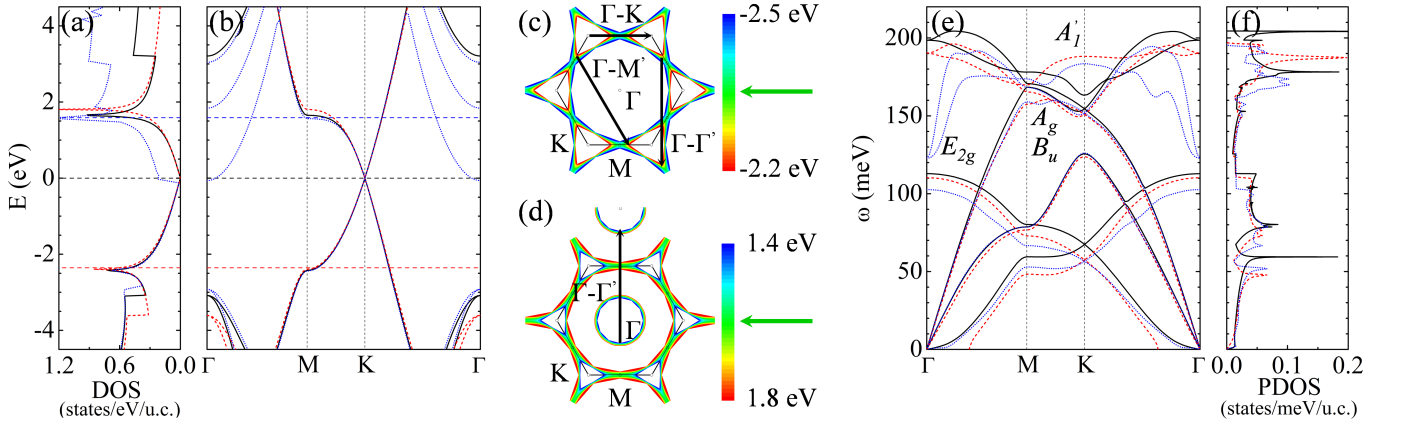


FIG. 1: (Color online) Electronic-structure and phonon-dispersion relations of pristine and doped graphene. (a) Electronic density of states and (b) band structures of pristine graphene (black solid line), *p*-doped graphene (dashed red line), and *n*-doped graphene (dotted blue line). (c),(d) Fermi surfaces of *p*-doped and *n*-doped graphene, respectively. In both cases, the Fermi surface corresponds to the green region of the energy isosurface, as indicated by the small arrow in the colorbar. The long black arrows indicate the dominant electron-phonon scattering mechanisms at the Fermi surface. (e) Phonon-dispersion relations of pristine, *p*-doped, and *n*-doped graphene, using the same color code as in (a). The vibrational modes discussed in the text are indicated. (f) Phonon density of states corresponding to the dispersions in (e).

II. MODELING DOPED GRAPHENE AT HIGH CARRIER DENSITY

In conventional superconductors the critical temperature increases with the electronic density of states at the Fermi level. In the case of graphene, this means that a best-case scenario for superconductivity should correspond to situations in which the Fermi level matches a VHS, either in the valence or in the conduction band. From our calculations, we find that the carrier densities required to approach the VHS are $0.8 \cdot 10^{15} \text{ cm}^{-2}$ for *p*-doped graphene, and $1.2 \cdot 10^{15} \text{ cm}^{-2}$ for *n*-doped graphene, respectively. Carrier densities near the VHS have been achieved via two-sided alkali metal doping of graphene²³, and densities up to $4 \cdot 10^{14} \text{ cm}^{-2}$ via electrolytic gating³². While carrier densities up to $3.5 \cdot 10^{15} \text{ cm}^{-2}$ have been demonstrated recently by means of polymer/electrolyte gating of gold thin films³³, such values may not be easily attainable in graphene due to its quantum capacitance^{34,35}.

Here we simulate carrier doping using a jellium model, whereby the excess/defect electronic charge is compensated by a uniform neutralizing background. This approximation has been used in previous studies to examine the effect of doping on the electronic bands, phonon dispersions, and EPC strength in carbon nanotubes^{38,39}, graphite intercalation compounds^{40,41}, and graphene^{16,42–47}. Besides being computationally advantageous, the jellium model is expected to provide a realistic description of graphene doped via electrochemical gating^{32,33}. In fact, while doping is expected to modify the band structure in proximity of the Dirac point^{36,37}, at high carrier densities its effects on the Fermi surface and the EPC are expected not to be significant. In the related

case of superconducting gated MoS_2 ⁴⁸, first-principles calculations using the same jellium model were able to reproduce the measured trends in the superconducting transition temperature⁴⁹. The calculations were carried out within the local density approximation to density-functional theory, using the codes **Quantum-ESPRESSO**⁵⁰, **EPW**⁵¹, and **Wannier90**⁵². The technical details of these calculations are described in Sec. VII at the end of this paper.

Figure 1 shows the calculated band structures, Fermi surfaces, and phonon-dispersion relations of pristine as well as doped graphene. In analogy with the interlayer state of graphite intercalation compounds, the FEL band crosses the Fermi level for *n*-doped graphene as shown in Fig. 1(b) (blue dotted lines). Upon doping, the highest optical phonon branches corresponding to the E_{2g} modes at Γ and the B_{3u} , B_{2u} , and A_g modes at M become softer, while the A'_1 mode at K hardens [Fig. 1(e)]. This behavior can be rationalized in terms of the changes intervening in the Fermi surface upon doping. In fact, it is well known that in pristine graphene the scattering of electrons around Γ and between Γ and K leads to two Kohn anomalies in the phonon dispersions at Γ and K ⁴². When graphene is doped until the Fermi level matches one of the VHS [Fig. 1(b)], the topology of the Fermi surface is dramatically altered and we obtain a hexagon connecting adjacent M points [Figs. 1(c) and 1(d)]. As a result, the Γ to K scattering channel is suppressed, while scattering between flat parallel sheets of the Fermi surface becomes possible, as shown schematically in Fig. 1(c) and (d). As a consequence, the original Kohn anomaly at K is lifted, and significant phonon softening is observed at Γ and M , corresponding with Γ - Γ' and Γ - M' scattering across adjacent Brillouin zones, respectively. We also

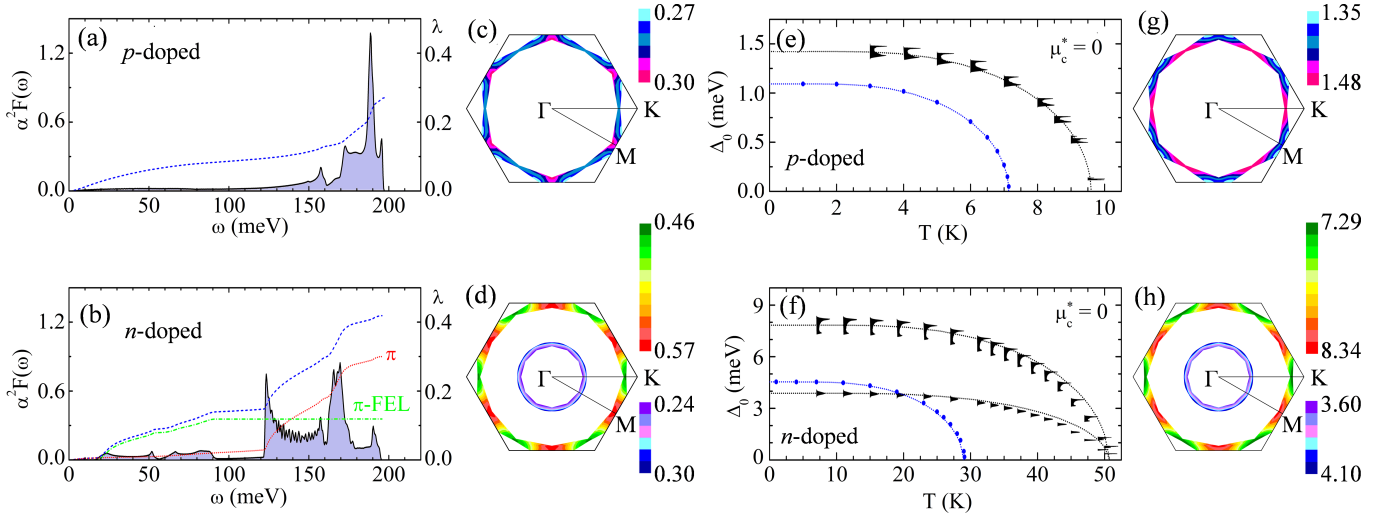


FIG. 2: (Color online) Electron-phonon coupling and superconducting gap function in doped graphene. (a), (b) Eliashberg spectral function and cumulative EPC calculated for *p*-doped and *n*-doped graphene, respectively. α^2F is the black solid line (left scale), $\lambda(\omega)$ is the blue dashed line (right scale). In the case of *n*-doped graphene we also show the decomposition of $\lambda(\omega)$ into contributions from the intraband π^* scattering (red dotted line) and interband π^* -FEL scattering (green dash-dotted line). (c), (d) Momentum-resolved EPC $\lambda_{\mathbf{k}}$ for electrons on the Fermi surface, for *p*-doped and *n*-doped graphene, respectively. (e)-(h) Anisotropic superconducting gap of *p*-doped graphene and *n*-doped graphene calculated using the Migdal-Eliashberg equations and $\mu_c^* = 0$. Panels (e) and (f) represent the energy distribution of the gap across the Fermi surface at various temperatures (shown in black), for *p*-doped and *n*-doped graphene, respectively. The isotropic superconducting gap is shown as blue filled dots. The dotted lines are BCS fits to the calculated data. Panels (g) and (h) show the corresponding superconducting gap at zero temperature on the Fermi surface (in meV). In the case of *n*-doped graphene, there are two superconducting gaps, one for the π^* band and one for the FEL band (h).

note that the softening of the lowest acoustic branch in *p*-doped graphene leads to a dynamical instability. This instability is expected to be mitigated by the coupling with a substrate; in any event, the soft mode does not contribute to the electron-phonon coupling in the following analysis.

In principle, the electron-hole symmetry around the Dirac point should result into similar Fermi surfaces for *p*-doping and *n*-doping. However, in the latter case the presence of a FEL band introduces an additional Fermi-surface sheet centered at Γ , as shown in Fig. 1(d). This extra sheet opens an additional Γ - Γ' scattering channel, and it is responsible for the more pronounced phonon softening near Γ in the case of *n*-doping. The details of the phonon softening/hardening upon doping are expected to change slightly when the lattice constant of doped graphene, non-adiabatic corrections⁴³, or the presence of dopant atoms are explicitly taken into account¹⁵. Nevertheless the general trends should be insensitive to these effects.

III. ELECTRON-PHONON INTERACTION IN HEAVILY DOPED GRAPHENE

Within the framework of conventional superconductivity, Cooper pairing arises from the interaction between electrons and phonons. In order to analyze the strength

of this interaction, in Fig. 2 we show the isotropic Eliashberg spectral function, $\alpha^2F(\omega)$, the cumulative EPC, $\lambda(\omega)$, and the momentum-resolved EPC of each electronic state at the Fermi surface, $\lambda_{\mathbf{k}}$. Here ω and \mathbf{k} represent the vibrational frequency and the electron momentum, respectively, and explicit expressions for $\alpha^2F(\omega)$, $\lambda(\omega)$, and $\lambda_{\mathbf{k}}$ are provided in Sec. VII.

Starting from *p*-doped graphene, $\lambda(\omega)$ displays a smooth increase as a function of phonon frequency, and the sharp peaks in $\alpha^2F(\omega)$ above 140 meV, corresponding to the optical modes, account for more than half of the total EPC, $\lambda = 0.27$ [Fig. 2(a)]. Fig. 2(c) shows that the momentum-resolved EPC is rather uniform across the Fermi surface, with $\lambda_{\mathbf{k}}$ varying smoothly in the range 0.27-0.30.

In the case of *n*-doped graphene, shown in Fig. 2(b), the Eliashberg function exhibits additional structure in the energy range 120-180 meV. By direct comparison with Fig. 1(e) this structure can be assigned to the large Kohn anomaly at Γ induced by doping. The softer phonons and the higher density of states at the Fermi level arising from the additional FEL band (1.01 for *n*-type doping vs. 0.62 states/eV/cell in the case of *p*-type doping) lead to a substantial increase of the total EPC with respect to *p*-doped graphene, up to $\lambda = 0.42$. In this case the optical phonons above 90 meV contribute almost two-thirds of the total EPC.

To clarify the role of the FEL band in *n*-doped

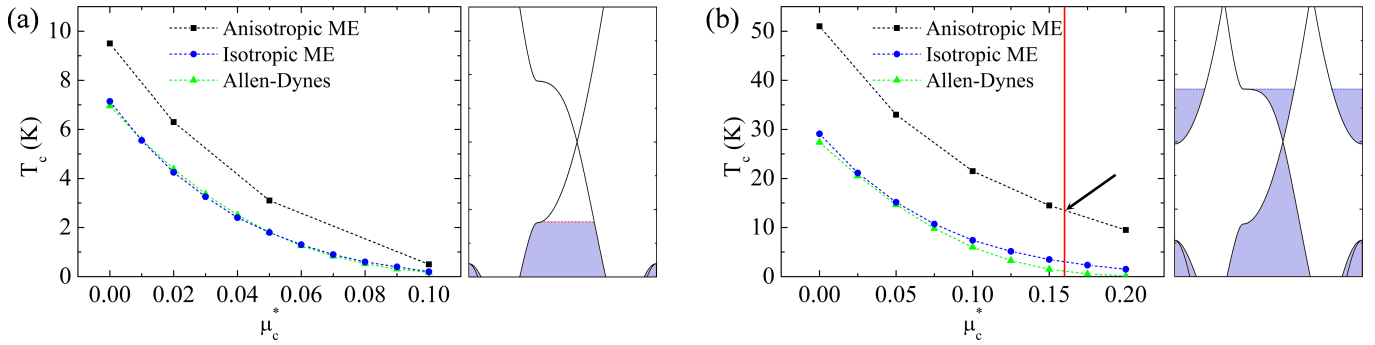


FIG. 3: (Color online) Superconducting critical temperature in doped graphene vs. Coulomb parameter. (a), (b) Calculated superconducting critical temperature as a function of the Coulomb pseudopotential μ_c^* , for p -doped graphene and n -doped graphene, respectively. The filled black squares are from anisotropic Migdal-Eliashberg calculations, the filled blue circles correspond to the isotropic approximation, and the filled green triangles are estimates based on the Allen-Dynes equation. The lines are guides to the eye. The vertical red line in (b) indicates the Coulomb parameter estimated here using the model dielectric function of Ref.⁶⁰, and the small arrow indicates our best estimate for the T_c of n -doped graphene. The schematic band-structure plots illustrate the two doping scenarios considered in this work.

graphene we show in Fig. 2(b) the contributions to $\lambda(\omega)$ associated with intraband scattering within the π^* sheet, and interband scattering between the π^* and FEL sheets. From this plot and the decomposition of $\lambda(\omega)$ into the contributions from each phonon mode, we deduce that the optical in-plane C-C stretching phonons are responsible for intraband scattering in the π^* sheet, while the out-of-plane buckling modes give rise to π^* -FEL interband scattering. The intraband scattering within the FEL sheet is found to be negligible. This phenomenology is similar to that of graphite-intercalation compounds⁴¹, however in the present case the π^* -FEL coupling is much smaller, due to the fact that the FEL wavefunction is located farther away from the graphene layer¹⁵. In agreement with these observations, Fig. 2(d) shows that the momentum-resolved coupling $\lambda_{\mathbf{k}}$ is relatively uniform on each Fermi surface sheet, but it differs considerably between the π^* sheet (0.46-0.57) and the FEL sheet (0.24-0.30).

IV. SUPERCONDUCTING PAIRING

Having examined the EPC in doped graphene we now move on to investigate its effect on the superconducting pairing. We solve the anisotropic Migdal-Eliashberg (ME) equations^{28,55,56} using the method described in Ref.²⁹. The solution to the ME equations, which are given explicitly in Sec. VII, provides the complete superconducting gap function $\Delta(\mathbf{k}, \omega)$ across the Fermi surface. From this quantity, the leading edge of the superconducting gap for electron momenta \mathbf{k} on the Fermi surface is obtained by solving for ω in $\Re \Delta(\mathbf{k}, \omega) = \omega$ ²⁹.

Since in the ME theory the Coulomb repulsion between electrons typically counters the electron-phonon pairing, as a best-case scenario we consider first the case of vanishing Coulomb pseudopotential, $\mu_c^* = 0$ (see Sec. VII). Figure 2 shows the calculated distribution of the leading

edge Δ_0 of the superconducting gap. In the case of p -doped graphene, the gap function is slightly anisotropic [anisotropy ratio $(\Delta_0^{\max} - \Delta_0^{\min})/\Delta_0^{\text{ave}} = 11\%$], however the symmetry is clearly s -wave as can be seen in Fig. 2(g). For a carrier density corresponding to 0.4 holes/cell we obtain a critical temperature $T_c(\mu_c^* = 0) = 9.5$ K and a ratio $2\Delta_0/k_B T_c = 3.44$, very close to the ideal BCS value of 3.53. The temperature dependence of the superconducting gap is well described by a BCS model, as obtained by solving numerically the BCS gap equation⁵³ using Δ_0 and T_c from our first-principles calculations. This is shown by the dotted black line in Fig. 2(e).

In the case of n -doped graphene, the presence of two Fermi surface sheets leads naturally to a two-gap structure, similar to the case of MgB_2 ⁵⁴⁻⁵⁶. As shown by Figs. 2(f) and 2(h), also in this case the gaps have s -wave symmetry and are slightly anisotropic. The calculated superconducting critical temperature is $T_c(\mu_c^* = 0) = 51$ K for a carrier density of 0.6 electrons/cell. In this case, the ratios between the gap and the critical temperature are $2\Delta_0^{\text{FEL}}/k_B T_c = 1.76$ and $2\Delta_0^{\pi^*}/k_B T_c = 3.57$, therefore it appears that the gap on the FEL sheet deviates substantially from the standard BCS behavior. Despite such a deviation our calculated distributions of superconducting gaps are described nicely by BCS curves, as shown by the dotted black lines in Fig. 2(f).

Interestingly, as we show in Fig. 2(e) and (f), if we neglect the anisotropy of the electron-phonon interaction, and solve instead the Eliashberg equations using the isotropic average of the Eliashberg function, then the resulting critical temperatures are severely underestimated, by up to a factor of 2. This finding indicates that the standard approach based on the Allen-Dynes equation⁵⁷, employed in all previous studies on graphene, is inadequate for studying superconductivity in this material. This observation is in line with similar analyses performed for superconducting MgB_2 ⁵⁶.

V. COULOMB EFFECTS

The results presented so far correspond to an ideal scenario whereby the electron-electron Coulomb interaction is assumed to have no effect on the superconducting pairing. To explore more realistic situations, we show in Fig. 3 the critical temperatures calculated for several values of the Coulomb pseudopotential μ_c^* in the typical range used for carbon materials¹⁶. As a direct consequence of the weak EPC in graphene, T_c varies strongly with μ_c^* . The trends shown in Fig. 3 are consistent with a simple analysis based on the Allen-Dynes equation⁵⁷ at variable μ_c^* (filled green triangles in Fig. 3). Since typical values for μ_c^* are in the range 0.10-0.20, we expect only *n*-doped graphene to exhibit superconductivity upon doping, with T_c of the order of 10 K.

It would be desirable to perform first principles calculations of the superconducting gap including electron-electron effects as in the density functional theory for superconductors (SCDFT)^{58,59}, however the incorporation of such effects in the ME theory is nontrivial. As a simpler alternative we estimate μ_c^* using the model screened Coulomb interaction proposed in Ref.⁶⁰ and the double Fermi surface average of Ref.⁶¹. Using this approach we estimate $\mu_c^* \simeq 0.16$, in good agreement with previous results¹⁶. The corresponding critical temperature for *n*-doped graphene is $T_c = 13$ K, as indicated by the vertical red line in Fig. 3(b). A detailed discussion of the parameter μ_c^* in a related system was given in Ref.⁶², where the Coulomb parameter of CaC_6 was determined by comparing the superconducting gap obtained from the ME theory and that from the SCDFT.

From this analysis it is clear that electron-electron interactions are important for the superconducting pairing in graphene. However, while in the context of the Eliashberg theory such interactions always tend to weaken the pairing, it is also possible that in proximity of a VHS novel Coulomb effects may emerge²³ and co-operate with the electron-phonon mechanism investigated here.

VI. CONCLUSIONS

In conclusion, we report the calculations of the superconducting properties of heavily doped graphene within the *ab initio* anisotropic Migdal-Eliashberg theory. Our work highlights the delicate interplay between electron-phonon interactions, anisotropy, and Coulomb effects in this material, and it demonstrates that simplified approaches based on isotropic approximations, such as the Allen-Dynes equation, are inadequate in this context.

Our main finding is that, when enough carriers are injected into graphene so that the Fermi level is aligned with the VHS in the π^* manifold, it should be possible to observe conventional superconductivity at low temperature, due to the extra pairing associated with the FEL band. In this case, two distinct superconducting gaps should be clearly observable in tunneling experi-

ments. Given the role of the FEL state in the superconductivity of *n*-doped graphene, and the well-known sensitivity of the FEL energetics to dielectric screening and quantum confinement^{38,63,64}, the superconducting state of graphene is expected to be rather delicate, and sensitive to device design and materials preparation.

We hope that this work will serve as a guideline to experimental research in the quest for a superconducting state that remains, to date, elusive.

VII. METHODS

The calculations are performed within the local density approximation (LDA) to density-functional theory^{65,66} and norm-conserving pseudopotentials^{67,68} using Quantum-ESPRESSO⁵⁰. The valence electronic wavefunctions are expanded in a plane-wave basis set with a kinetic energy cutoff of 60 Ry. A graphene layer in isolation is described using a supercell geometry. The optimized lattice parameter is $a = 2.434$ Å and periodic replicas are 10 Å apart. The electron charge density is computed using a Γ -centered Brillouin-zone mesh with $72 \times 72 \times 1$ \mathbf{k} -points and a Methfessel-Paxton smearing⁶⁹ of 0.10 eV. The dynamical matrices and the linear variation of the self-consistent potential are calculated within density-functional perturbation theory⁷⁰ on the irreducible set of a regular $12 \times 12 \times 1$ \mathbf{q} -point mesh. The electronic wavefunctions required for the Wannier-Fourier interpolation within the EPW code^{30,51} are calculated on a uniform and Γ -centered \mathbf{k} -points mesh of size $12 \times 12 \times 1$. We considered seven maximally-localized Wannier functions^{31,52} in order to describe the electronic band structure up to 1 eV above the VHS in the conduction band. Two Wannier functions are p_z -like states (one per C atom), three functions are σ -like states localized in the middle of C-C bonds, and two correspond to s -like states located directly above and below the center of the C_6 hexagon. We consider two doping scenarios where the Fermi energy matches either one of the two VHS in the π or π^* manifolds. This is achieved by using 0.4 electrons per unit cell ($0.8 \cdot 10^{15} \text{ cm}^{-2}$) for *p*-doped graphene, and 0.6 electrons per unit cell ($1.2 \cdot 10^{15} \text{ cm}^{-2}$) for *n*-doped graphene. The isotropic Eliashberg spectral function is defined as:

$$\alpha^2 F(\omega) = \frac{1}{N_F N_{\mathbf{k}} N_{\mathbf{q}}} \sum_{\mathbf{k}, \mathbf{k}', \nu} |g_{\mathbf{k}\mathbf{k}'}^\nu|^2 \delta(\epsilon_{\mathbf{k}}) \delta(\epsilon_{\mathbf{k}'}) \delta(\omega - \omega_{\mathbf{q}\nu}), \quad (1)$$

the cumulative EPC is calculated as²⁸:

$$\lambda(\omega) = 2 \int_0^\omega d\omega' \alpha^2 F(\omega') / \omega', \quad (2)$$

and the momentum-resolved EPC of each electronic state at the Fermi surface is given by²⁹:

$$\lambda_{\mathbf{k}} = \sum_{\mathbf{k}', \nu} \delta(\epsilon_{\mathbf{k}'}) |g_{\mathbf{k}\mathbf{k}'}^\nu|^2 / \omega_{\mathbf{q}\nu}. \quad (3)$$

In these expressions N_F represents the density of electronic states per spin at the Fermi level, $N_{\mathbf{k}}$ and $N_{\mathbf{q}}$ are the total numbers of \mathbf{k} and \mathbf{q} points, $\epsilon_{\mathbf{k}}$ is the Kohn-Sham eigenvalue referred to the Fermi level, and $g'_{\mathbf{k}\mathbf{k}'}$ is the screened electron-phonon matrix element for the scattering between the electronic states \mathbf{k} and \mathbf{k}' through a phonon with wave vector $\mathbf{q} = \mathbf{k}' - \mathbf{k}$, frequency $\omega_{\mathbf{q}\nu}$ and branch index ν . Here \mathbf{k} and \mathbf{k}' indicate both the electron wavevector and the band index. The anisotropic Migdal-Eliashberg equations^{28,29,55,56} are given by:

$$Z(\mathbf{k}, i\omega_n) = 1 + \frac{\pi T}{N_F \omega_n} \sum_{\mathbf{k}'n'} \frac{\omega_{n'}}{\sqrt{\omega_{n'}^2 + \Delta^2(\mathbf{k}', i\omega_{n'})}} \times \delta(\epsilon_{\mathbf{k}'}) \lambda(\mathbf{k}, \mathbf{k}', n - n'), \quad (4)$$

$$Z(\mathbf{k}, i\omega_n) \Delta(\mathbf{k}, i\omega_n) = \frac{\pi T}{N_F} \sum_{\mathbf{k}'n'} \frac{\Delta(\mathbf{k}', i\omega_{n'})}{\sqrt{\omega_{n'}^2 + \Delta^2(\mathbf{k}', i\omega_{n'})}} \times \delta(\epsilon_{\mathbf{k}'}) [\lambda(\mathbf{k}, \mathbf{k}', n - n') - \mu_c^*]. \quad (5)$$

Here $\omega_n = (2n + 1)\pi T$ with n integer are fermion Matsubara frequencies, and T is the absolute temperature.

$Z(\mathbf{k}, i\omega_n)$ is the mass renormalization function, $\Delta(\mathbf{k}, i\omega_n)$ is the superconducting gap function, $\lambda(\mathbf{k}, \mathbf{k}', n - n')$ is the momentum- and energy-dependent EPC, and μ_c^* is the semiempirical Coulomb parameter. From the superconducting gap function $\Delta(\mathbf{k}, i\omega_n)$ we obtain the gap at real-valued frequencies via Padé approximants^{71,72}. A detailed discussion of the formalism can be found in Ref.²⁹. For the solution of the Eliashberg equations it is absolutely critical to use extremely fine Brillouin-zone grids²⁹. In this study we use grids containing $400 \times 400 \times 1$ \mathbf{k} -points and $200 \times 200 \times 1$ \mathbf{q} -points, respectively. The frequency cutoff in the Migdal-Eliashberg equations is set to five times the maximum phonon frequency, and the Dirac delta functions are smeared using Lorentzian broadenings of 100 meV and 0.5 meV for electrons and phonons, respectively. All the technical details of the Migdal-Eliashberg calculations are described extensively in Ref.²⁹.

F.G. acknowledges support from the European Research Council (EU FP7/ERC grant no. 239578 and EU FP7/grant no. 604391 Graphene Flagship) and the Leverhulme Trust (Grant RL-2012-001).

* Electronic address: rmargine@binghamton.edu

† Electronic address: feliciano.giustino@materials.ox.ac.uk

¹ N. B. Hannay, T. H. Geballe, B. T. Matthias, K. Andres, P. Schmidt, and D. MacNair, Superconductivity in graphitic compounds, *Phys. Rev. Lett.* **14**, 225 (1965).

² T. E. Weller, M. Ellerby, S. S. Saxena, R. P. Smith, and N. T. Skipper, Superconductivity in the intercalated graphite compounds C_6Yb and C_6Ca , *Nat. Phys.* **1**, 39 (2005).

³ A. Y. Ganin, Y. Takabayashi, Y. Z. Khimiyak, S. Margadonna, A. Tamai, M. J. Rosseinsky, and K. Prassides, Bulk superconductivity at 38 K in a molecular system, *Nat. Mater.* **7**, 367 (2008).

⁴ E. A. Ekimov, V. A. Sidorov, E. D. Bauer, N. N. Mel'nik, N. J. Curro, J. D. Thompson, and S. M. Stishov, Superconductivity in diamond, *Nature (London)* **428**, 542 (2004).

⁵ Y. Takano, T. Takenouchi, S. Ishii, S. Ueda, T. Okutsu, I. Sakaguchi, H. Umezawa, H. Kawarada, and M. Tachiki, Superconducting properties of homoepitaxial CVD diamond, *Diamond Relat. Mater.* **16**, 911 (2007).

⁶ R. Mitsunashi, Y. Suzuki, Y. Yamanari, H. Mitamura, T. Kambe, N. Ikeda, H. Okamoto, A. Fujiwara, M. Yamaji, N. Kawasaki, Y. Maniwa, and Y. Kubozono, Superconductivity in alkali-metal-doped picene, *Nature (London)* **464**, 76 (2010).

⁷ X. F. Wang, R. H. Liu, Z. Gui, Y. L. Xie, Y. J. Yan, J. J. Ying, X. G. Luo, and X. H. Chen, Superconductivity at 5 K in alkali-metal-doped phenanthrene, *Nat. Commun.* **2**, 507 (2011).

⁸ Y. Kubozono, H. Mitamura, X. Lee, X. He, Y. Yamanari, Y. Takahashi, Y. Suzuki, Y. Kaji, R. Eguchi, K. Akaike, T. Kambe, H. Okamoto, A. Fujiwara, T. Kato, T. Kosugi, and H. Aoki, Metal-intercalated aromatic hydrocarbons: a new class of carbon-based superconductors, *Phys. Chem. Chem. Phys.* **13**, 16476 (2011).

⁹ M. Xue, T. Cao, D. Wang, Y. Wu, H. Yang, X. Dong, J.

He, F. Li, and G. F. Chen, Superconductivity above 30 K in alkali-metal-doped hydrocarbon, *Sci. Rep.* **2**, 389 (2012).

¹⁰ K. S. Novoselov, A. K. Geim, S. V. Morozov, D. Jiang, Y. Zhang, S. V. Dubonos, I. V. Grigorieva, and A. A. Firsov, Electric field effect in atomically thin carbon films, *Science* **306**, 666 (2004).

¹¹ K. S. Novoselov, D. Jiang, F. Schedin, T. J. Booth, V. V. Khotkevich, S. V. Morozov, and A. K. Geim, Two-dimensional atomic crystals, *Proc. Natl. Acad. Sci. (U.S.A.)* **102**, 10451 (2005).

¹² A. H. Castro Neto, F. Guinea, N. M. R. Peres, K. S. Novoselov, and A. K. Geim, The electronic properties of graphene, *Rev. Mod. Phys.* **81**, 109 (2009).

¹³ F. Bonaccorso, Z. Sun, T. Hasan, and A. C. Ferrari, Graphene photonics and optoelectronics, *Nat. Photonics* **4**, 611 (2010).

¹⁴ M. Einenkel and K. B. Efetov, Possibility of superconductivity due to electron-phonon interaction in graphene, *Phys. Rev. B* **84**, 214508 (2011).

¹⁵ G. Profeta, M. Calandra, and F. Mauri, Phonon-mediated superconductivity in graphene by lithium deposition, *Nat. Phys.* **8**, 131 (2012).

¹⁶ C. Si, Z. Liu, W. Duan, and F. Liu, First-Principles calculations on the effect of doping and biaxial tensile strain on electron-phonon coupling in graphene, *Phys. Rev. Lett.* **111**, 196802 (2013).

¹⁷ B. Uchoa and A. H. Castro Neto, Superconducting states of pure and doped graphene, *Phys. Rev. Lett.* **98**, 146801 (2007).

¹⁸ R. Nandkishore, L. S. Levitov, and A. V. Chubukov, Chiral superconductivity from repulsive interactions in doped graphene, *Nat. Phys.* **8**, 158 (2012).

¹⁹ M. L. Kiesel, C. Platt, W. Hanke, D. A. Abanin, and R. Thomale, Competing many-body instabilities and unconventional superconductivity in graphene, *Phys. Rev. B* **86**,

- 020507(R) (2012).
- ²⁰ J. O. Sofo, A. S. Chaudhari, and G. D. Barber, Graphane: A two-dimensional hydrocarbon, *Phys. Rev. B* **75**, 153401 (2007).
 - ²¹ G. Savini, A. C. Ferrari, and F. Giustino, First-principles prediction of doped graphane as a high-temperature electron-phonon superconductor, *Phys. Rev. Lett.* **105**, 037002 (2010).
 - ²² N. D. Mermin and H. Wagner, Absence of ferromagnetism or antiferromagnetism in one- or two-dimensional isotropic Heisenberg models, *Phys. Rev. Lett.* **17**, 1133 (1966).
 - ²³ J. L. McChesney, A. Bostwick, T. Ohta, T. Seyller, K. Horn, J. González, and Eli Rotenberg, Extended van Hove singularity and superconducting instability in doped graphene, *Phys. Rev. Lett.* **104**, 136803 (2010).
 - ²⁴ M. Bianchi, E. D. L. Rienks, S. Lizzit, A. Baraldi, R. Balog, L. Hornekær, and P. Hofmann, Electron-phonon coupling in potassium-doped graphene: Angle-resolved photoemission spectroscopy, *Phys. Rev. B* **81**, 041403 (2010).
 - ²⁵ D. A. Siegel, C. Hwang, A. V. Fedorov, and A. Lanzara, Electron-phonon coupling and intrinsic bandgap in highly-screened graphene, *New J. Phys.* **14**, 095006 (2012).
 - ²⁶ D. Haberer, L. Petaccia, A. V. Fedorov, C. S. Praveen, S. Fabris, S. Piccinin, O. Vilkov, D. V. Vyalikh, A. Preobrazhenski, N. I. Verbitskiy, H. Shiozawa, J. Fink, M. Knupfer, B. Büchner, and A. Grüneis, Anisotropic Eliashberg function and electron-phonon coupling in doped graphene, *Phys. Rev. B* **88**, 081401 (2013).
 - ²⁷ S. Y. Zhou, G.-H. Gweon, A. V. Fedorov, P. N. First, W. A. de Heer, D.-H. Lee, F. Guinea, A. H. Castro Neto, and A. Lanzara, Substrate-induced bandgap opening in epitaxial graphene, *Nat. Mater.* **6**, 770 (2007).
 - ²⁸ P. B. Allen and B. Mitrović, Theory of superconducting T_c , *Solid State Phys.* **37**, 1 (1982).
 - ²⁹ E. R. Margine and F. Giustino, Anisotropic Migdal-Eliashberg theory using Wannier functions, *Phys. Rev. B* **87**, 024505 (2013).
 - ³⁰ F. Giustino, M. L. Cohen, and S. G. Louie, Electron-phonon interaction using Wannier functions, *Phys. Rev. B* **76**, 165108 (2007).
 - ³¹ N. Marzari, A. A. Mostofi, J. R. Yates, I. Souza, and D. Vanderbilt, Maximally localized Wannier functions: Theory and applications, *Rev. Mod. Phys.* **84**, 1419 (2012).
 - ³² D. K. Efetov and P. Kim, Controlling electron-phonon interactions in graphene at ultrahigh carrier densities *Phys. Rev. Lett.* **105**, 256805 (2010).
 - ³³ D. Daghero, F. Paolucci, A. Sola, M. Tortello, G. A. Ummarino, M. Agosto, R. S. Gonnelli, J. R. Nair, and C. Gerbaldi, Large conductance modulation of gold thin films by huge charge injection via electrochemical gating, *Phys. Rev. Lett.* **108**, 066807 (2012).
 - ³⁴ J. Ye, M. F. Craciun, M. Koshino, S. Russo, S. Inoue, H. Yuan, H. Shimotani, A. F. Morpurgo, and Y. Iwasa, Accessing the transport properties of graphene and its multilayers at high carrier density, *Proc. Natl. Acad. Sci.* **108**, 13002 (2011).
 - ³⁵ E. Uesugi, H. Goto, R. Eguchi, A. Fujiwara, and Y. Kubozono, Electric double-layer capacitance between an ionic liquid and few-layer graphene, *Sci. Rep.* **3**, 1595 (2013).
 - ³⁶ M. F. Craciun, S. Russo, M. Yamamoto, and S. Tarucha, Tuneable electronic properties in graphene, *Nano Today* **6**, 42 (2011) and references there in.
 - ³⁷ C. H. Lui, Z. Li, K. F. Mak, E. Cappelluti, and T. F. Heinz, Observation of an electrically tunable band gap in trilayer graphene, *Nat. Phys.* **7**, 944 (2011).
 - ³⁸ E. R. Margine and V. H. Crespi, Universal behavior of nearly free electron states in carbon nanotubes, *Phys. Rev. Lett.* **96**, 196803 (2006).
 - ³⁹ E. R. Margine, P. E. Lammert, and V. H. Crespi, Reciprocal space constraints create real-space anomalies in doped carbon nanotubes, *Phys. Rev. Lett.* **99**, 196803 (2007).
 - ⁴⁰ G. Csányi, P. B. Littlewood, A. H. Nevidomskyy, C. H. Pickard, and B. D. Simons, The role of the interlayer state in the electronic structure of superconducting GICs, *Nature Physics* **1**, 42 (2005).
 - ⁴¹ L. Boeri, G. B. Bachelet, M. Giantomassi, and O. K. Andersen, Electron-phonon interaction in graphite intercalation compounds, *Phys. Rev. B* **76**, 064510 (2007).
 - ⁴² S. Piscanec, M. Lazzeri, F. Mauri, A. C. Ferrari, and J. Robertson, Kohn anomalies and electron phonon interactions in graphite, *Phys. Rev. Lett.* **93**, 185503 (2004).
 - ⁴³ M. Lazzeri and F. Mauri, Nonadiabatic Kohn anomaly in a doped graphene monolayer, *Phys. Rev. Lett.* **97**, 266407 (2006).
 - ⁴⁴ C.-H. Park, F. Giustino, M. L. Cohen, and S. G. Louie, Velocity renormalization and carrier lifetime in graphene from the electron-phonon interaction, *Phys. Rev. Lett.* **99**, 086804 (2007).
 - ⁴⁵ C.-H. Park, F. Giustino, J. L. McChesney, A. Bostwick, T. Ohta, E. Rotenberg, M. L. Cohen, and S. G. Louie, Van Hove singularity and apparent anisotropy in the electron-phonon interaction in graphene, *Phys. Rev. B* **77**, 113410 (2008).
 - ⁴⁶ M. Calandra and F. Mauri, Electron-phonon coupling and electron self-energy in electron-doped graphene: Calculation of angular-resolved photoemission spectra, *Phys. Rev. B* **76**, 205411 (2007).
 - ⁴⁷ C.H. Park, F. Giustino, M. L. Cohen, and S. G. Louie, Electron-Phonon Interactions in graphene, bilayer graphene, and graphite, *Nano Lett.* **8**, 4229 (2008).
 - ⁴⁸ J. T. Ye, Y. J. Zhang, R. Akashi, M. S. Bahramy, R. Arita, and Y. Iwasa, Superconducting dome in a gate-tuned band insulator, *Science* **338**, 1193 (2012).
 - ⁴⁹ Y. Ge and A. Y. Liu, Phonon-mediated superconductivity in electron-doped single-layer MoS_2 : A first-principles prediction, *Phys. Rev. B* **87**, 241408(R) (2013).
 - ⁵⁰ P. Giannozzi *et al.*, QUANTUM ESPRESSO: a modular and open-source software project for quantum simulations of materials, *J. Phys. Condens. Matter* **21**, 395502 (2009).
 - ⁵¹ J. Noffsinger, F. Giustino, B. D. Malone, C.-H. Park, S. G. Louie, and M. L. Cohen, EPW: A program for calculating the electronphonon coupling using maximally localized Wannier functions, *Comput. Phys. Commun.* **181**, 2140 (2010).
 - ⁵² A. A. Mostofi, J. R. Yates, Y.-S. Lee, I. Souza, D. Vanderbilt, and N. Marzari, wannier90: A tool for obtaining maximally-localised Wannier functions, *Comput. Phys. Comm.* **178**, 685 (2008).
 - ⁵³ J. Bardeen, L. N. Cooper, and J. R. Schrieffer, Theory of superconductivity, *Phys. Rev.* **108**, 1175 (1957).
 - ⁵⁴ A. Y. Liu, I. I. Mazin, and J. Kortus, *Phys. Rev. Lett.* **87**, 087005 (2001).
 - ⁵⁵ H. J. Choi, D. Roundy, H. Sun, M. L. Cohen, and S. G. Louie, The origin of the anomalous superconducting properties of MgB_2 , *Nature (London)* **418**, 758 (2002).
 - ⁵⁶ H. J. Choi, D. Roundy, H. Sun, M. L. Cohen, and S. G. Louie, First-principles calculation of the superconducting transition in MgB_2 within the anisotropic Eliashberg for-

- malism, Phys. Rev. B **66**, 020513(R) (2002).
- ⁵⁷ P. B. Allen and R. C. Dynes, Transition temperature of strong-coupled superconductors reanalyzed, Phys. Rev. B **12**, 905 (1975).
 - ⁵⁸ M. Lüders, M. A. L. Marques, N. N. Lathiotakis, A. Floris, G. Profeta, L. Fast, A. Continenza, S. Massidda, and E. K. U. Gross, Ab initio theory of superconductivity. I. Density functional formalism and approximate functionals, Phys. Rev. B **72**, 024545 (2005).
 - ⁵⁹ M. A. L. Marques, M. Lüders, N. N. Lathiotakis, G. Profeta, A. Floris, L. Fast, A. Continenza, E. K. U. Gross, and S. Massidda, Ab initio theory of superconductivity. II. Application to elemental metals Phys. Rev. B **72**, 024546 (2005).
 - ⁶⁰ E. H. Hwang and S. Das Sarma, Dielectric function, screening, and plasmons in two-dimensional graphene, Phys. Rev. B **75**, 205418 (2007).
 - ⁶¹ K.-H. Lee, K. J. Chang, and M. L. Cohen, First-principles calculations of the Coulomb pseudopotential μ^* : Application to Al, Phys. Rev. B **52**, 1425 (1995).
 - ⁶² A. Sanna, S. Pittalis, J. K. Dewhurst, M. Monni, S. Sharma, G. Umrigar, S. Massidda, and E. K. U. Gross, Phononic self-energy effects and superconductivity in CaC_6 , Phys. Rev. B **85**, 184514 (2012).
 - ⁶³ M. Topsakal and S. Ciraci, Static charging of graphene and graphite slabs, Appl. Phys. Lett. **98**, 131908 (2011).
 - ⁶⁴ M. Topsakal and S. Ciraci, Effects of static charging and exfoliation of layered crystals, Phys. Rev. B **85**, 045121 (2012).
 - ⁶⁵ D. M. Ceperley and B. J. Alder, Ground state of the electron gas by a stochastic method, Phys. Rev. Lett. **45**, 566 (1980).
 - ⁶⁶ J. P. Perdew and A. Zunger, A self-interaction correction to density-functional approximations for many-electron systems, Phys. Rev. B **23**, 5048 (1981).
 - ⁶⁷ N. Troullier and J. L. Martins, Efficient pseudopotentials for plane-wave calculations, Phys. Rev. B **43**, 1993 (1991).
 - ⁶⁸ M. Fuchs and M. Scheffler, Ab initio pseudopotentials for electronic structure calculations of poly-atomic systems using density-functional theory, Comput. Phys. Commun. **119**, 67 (1999).
 - ⁶⁹ M. Methfessel and A. T. Paxton, High-precision sampling for Brillouin-zone integration in metals, Phys. Rev. B **40**, 3616 (1989).
 - ⁷⁰ S. Baroni, S. de Gironcoli, A. Dal Corso, and P. Gianozzi, Phonons and related crystal properties from density-functional perturbation theory, Rev. Mod. Phys. **73**, 515 (2001).
 - ⁷¹ H. J. Vidberg and J. W. Serene, Solving the Eliashberg Equations by Means of N-Point Padé Approximants, J. Low Temp. Phys. **29**, 179 (1977).
 - ⁷² C. R. Leavens and D. S. Ritchie, Extension of the N-point Padé approximants solution of the Eliashberg equations to $T \approx T_c$, Solid State Commun. **53**, 137 (1985).